Polymer 340 (2025) 129131

Contents lists available at ScienceDirect

Polymer

journal homepage: www.elsevier.com/locate/polymer

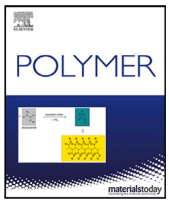

Intracrystalline chain diffusion, semicrystalline morphology and mechanical modulus of selected aliphatic polyesters☆

Yu Qiang [a], Afiq Anuar [a], Aaron Miller [a], Sharifa Abdullaeva [a], Katalee Jariyavidyanont [a], Albrecht Petzold [a], Svenja Stürmer [b], Felix Scheliga [b], Kay Saalwächter [a,*], Thomas Thurn-Albrecht [a,*]

[a] Institut für Physik, Martin-Luther-Universität Halle-Wittenberg, Halle (Saale), 06099, Germany
[b] Institut für Technische und Makromolekulare Chemie, Universität Hamburg, Hamburg, 20146, Germany

ARTICLE INFO

Dataset link: https://doi.org/10.5281/zenodo.15648710

Keywords:
Polymer crystallization
Intracrystalline chain diffusion
Semicrystalline morphology
Crystal thickening
Mechanical properties
Aliphatic polyesters

ABSTRACT

Recently, based upon experiments on three model polymers, we concluded that semicrystalline polymers exhibit different morphological features depending on the timescale of intracrystalline chain diffusion (ICD) relative to the kinetics of crystal growth. In this study, we investigated a series of selected aliphatic polyesters to test the generality of this concept. ICD and crystallization kinetics of the selected polyesters were characterized by nuclear magnetic resonance (NMR) and optical microscopy, respectively. Small-angle X-ray scattering (SAXS) was used to reveal the semicrystalline morphology, and to differentiate ICD of polyesters with rather slow ICD (undetectable by NMR) through comparing crystal-thickening slopes during crystallization. Our results confirm that the observed relation between morphology and ICD is valid for all investigated polyesters. The formation of ester layers in the polyester crystals results in slowing down of ICD and a reduction of the enthalpy of melting ($\Delta H_{m,100}$), which is determined via a reliable combination of differential scanning calorimetry with ^{1}H low-resolution NMR and further confirmed by SAXS. In addition, we propose a further refinement and expansion of the classification of the crystal-fixed polymers, a term that is commonly used in the literature. Furthermore, the shear modulus of the selected polyesters with slow ICD shows a common exponential dependence on their crystallinity.

1. Introduction

The nanoscopic morphology of semicrystalline polymers consists of stacks of thin lamellar crystals separated by amorphous layers, which plays an important role in determining their macroscopic mechanical properties [1]. It was observed by Boyd [2,3] that this semicrystalline morphology is closely related to intracrystalline chain diffusion (ICD). ICD is a unique feature of semicrystalline polymers and refers to the mobility of polymer chains in and through the crystallites [4,5]. This process is associated with a crystalline α-relaxation (α_c-relaxation) [5], a thermally activated process requiring a specific activation energy [5], which corresponds to the average time between two monomer jumps. This can be quantitatively characterized by nuclear magnetic resonance (NMR) measurements up to 1 s [4–8]. The α_c-relaxation can also be observed via dynamic mechanical analysis (DMA) [2,9–11] and other measurements [2]. The corresponding activation energy of this α_c-relaxation can be determined by NMR or DMA methods with the Arrhenius equation [9,10,12].

Our recent studies on semicrystalline morphology, based on a few model polymers, show that the timescale of ICD ($\langle\tau_c\rangle$) relative to the kinetics of crystal growth (τ_{lc}) determines the fundamental morphological feature of semicrystalline polymers [4,12,13]. When $\langle\tau_c\rangle$ is much longer than τ_{lc}, the polymers are referred to "crystal-fixed" polymers. These polymers, such as polycaprolactone (PCL), exhibit no or only rather slow ICD, which cannot be further resolved by NMR measurements [4]. They show morphological features where the thickness of crystalline layer (d_c) is comparable to or smaller than that of amorphous layer (d_a), and the distribution width of d_c (σ_c) is much narrower than that of d_a (σ_a) at the crystallization temperature (T_c). The morphological features (d_a, d_c, σ_a, σ_c) can be characterized by quantitative modeling of SAXS data [12,14]. In addition, insertion crystallization takes place in crystal-fixed polymers, i.e. upon cooling thin crystals form (from T_c to lower temperature) in the large amorphous regions, which can be measured quantitatively by NMR

☆ This article is part of a Special issue entitled: 'Honoring C. De Rosa' published in Polymer.

* Corresponding authors.
E-mail addresses: kay.saalwaechter@physik.uni-halle.de (K. Saalwächter), thomas.thurn-albrecht@physik.uni-halle.de (T. Thurn-Albrecht).

https://doi.org/10.1016/j.polymer.2025.129131
Received 30 June 2025; Received in revised form 8 September 2025; Accepted 22 September 2025
Available online 16 October 2025

measurement and further confirmed by the combination of SAXS and WAXS measurements [1,12,13]. In contrast, when $\langle\tau_c\rangle$ is comparable to or shorter than τ_{lc}, the polymers are termed as "crystal-mobile" polymers. These polymers, e.g. high density polyethylene (HDPE) and polyethyleneoxide (PEO), possess fast ICD (short $\langle\tau_c\rangle$), which is clearly detected by NMR measurements. They demonstrate opposing morphological features to that of crystal-fixed polymer: d_a is much thinner than d_c, and σ_a is significantly narrower than σ_c at crystallization temperatures (T_c). Upon cooling, instead of insertion crystallization, crystal-mobile polymers tend to form crystals through post-growth thickening, also referred to as surface crystallization [15], which occurs mostly at the interface between crystalline and amorphous regions and does not significantly increase crystallinity [12].

Although PCL, a polyester, is classified as a "crystal-fixed" polymer, we still noticed slow crystal thickening during secondary crystallization [4], a process typically related to the existence of ICD. While during insertion crystallization new thinner crystals form, a thickening during secondary crystallization cannot be caused by the formation of new thicker crystals, simply as there is not enough space available in the already formed crystal stacks. As mentioned above, it is possible that PCL possesses rather slow ICD instead of being strictly crystal-fixed, a distinction that remains challenging to resolve. Polyesters are generally classified as crystal-fixed polymers in polymer physics textbooks [16], as these materials typically meet the typical molecular criteria (e.g. with pendant groups and long monomer units) that impede ICD. However, notable exceptions exist. Poly-L-lactic acid (PLLA) and poly-3-hydroxylbutyrate (P3HB), two commercially available polyesters, exhibit crystal-mobile behavior [10,17]. In addition, a copolyester of polycaprolactone and polypentadecalactone (PCL-co-PPDL), which contains rather long monomer units, exhibits the α_c-relaxation associated with ICD [18]. Song et al. proposed that a helical chain conformation in the crystals, as opposed to a planar conformation, facilitates ICD [19]. However, this hypothesis is contradictory to the case of a well-known crystal-mobile polymer, high-density polyethylene (HDPE), which adopts planar chain conformation [20]. Marxsen et al. [21] showed that a layered ester structure is present in the polyester crystals, which has been demonstrated to hinder ICD [18].

Following these observations, and considering that both the α_c-relaxation (or ICD) and semicrystalline morphology (crystal content-crystallinity) both have significant influence on mechanical modulus of polymers [11,22], we aim to investigate the influence of ester groups on the intracrystalline chain diffusion (ICD) by studying a series of aliphatic polyesters with systematically varied ester content. Although some aliphatic polyesters are already commercially available and widely used [23–26], their intracrystalline chain diffusion (ICD) and semicrystalline morphology are not yet fully studied, not to mention other aliphatic polyesters. Thus, we want to characterize their ICD and semicrystalline morphology and check the generality of our hypothesis about the dependence of semicrytalline morphology on the relative of the timescale of ICD and layer crystallization. In addition, we aim to explore the possibility of distinguishing differences in the timescale of ICD among crystal-fixed polymers. Furthermore, mechanical properties specifically the shear modulus, which is closely related to both ICD and semicrystalline morphology, will be systematically investigated due to their importance for practical applications.

We therefore present here an experimental study of selected aliphatic polyesters with various ester content using a combination of solid-state NMR and SAXS-based analysis to estimate the timescale of ICD and complete semicrystalline morphology. A newly developed approach based on SAXS was used to differentiate ICDs among crystal-fixed polymers with different ester content. Reliable values for enthalpy of melting ($\Delta H_{m,100}$) of the selected polyesters are reported based on the robust techniques: solid-state NMR techniques and differential scanning calorimetry (DSC). In addition, we report the dependence of shear modulus on semicrystalline morphology (crystallinity) and ICD.

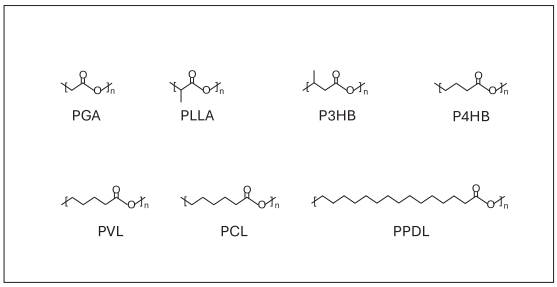

Fig. 1. Chemical structures of the monomers of the selected polyesters: PGA (poly glycolic acid), PLLA (poly-L-lactide acid), P3HB (poly-3-hydroxybutyrate), P4HB (Poly-4-hydroxybutyrate), PVL (polyvalerolactone), PCL (polycaprolactone), PPDL (poly ω-pentadecalactone).

As aliphatic polyesters are promising alternatives to commodity plastics such as polyethylene (PE) and polypropylene (PP) due to their similar mechanical and thermal properties and combined with recyclability and degradability [27,28], a thorough fundamental understanding from chemical structure to microstructure and macroscopic properties is essential for guiding material design and future applications.

2. Experimental section

2.1. Materials

We selected the series of aliphatic polyesters, within the constraints of material availability, with the main aim to cover a broad range of N_{cc}. N_{cc} is the number of carbon–carbon bonds in the monomer along the backbone, namely the length of methylene sequence in the monomer if there is no side chain. The chemical structures of the monomers are illustrated in Fig. 1. Poly glycolic acid (PGA) was purchased from Polysciences Europe GmbH (Germany). The molecular weight (M_w) is above $100\,kg\,mol^{-1}$. Poly-L-lactide acid (PLLA) was provided by Corbion (Amsterdam, Netherlands) in the form of pellets (Grade: L175), with M_w of $120\,kg\,mol^{-1}$. Poly-3-hydroxybutyrate (P3HB) was supplied by Dr. Hänggi from Biomer (Germany), in the form of pellets (P338) from T26 powder. Poly-4-hydroxybutyrate (P4HB) was synthesized by Prof. Manfred Zinn from HES-SO Valais-Wallis university (Switzerland). Polyvalerolactone (PVL) was synthesized by Dr. Svenja Stürmer from university Hamburg, with $M_w = 190\,kg\,mol^{-1}$, PDI = 2. Poly ω-pentadecalactone (PPDL) was provided by Dr. Felix Scheliga from university Hamburg, $M_w = 439\,kg\,mol^{-1}$, PDI=4.92. In addition, the high density polyethylene (HDPE) and polybutylene succinate (PBS) used in this study as benchmark materials were provided by Total (Grade: Lumicene® mPE M5510EP) with $M_n = 27\,700\,g\,mol^{-1}$, PDI = 2.8 and by PTT MCC Biochem Co., Ltd. (Grade: FZ91) with $M_n = 40\,850\,g\,mol^{-1}$, $M_w = 143\,400\,g\,mol^{-1}$. Further detailed information of the samples can be found in Table 1. The melting temperatures of the different samples vary over a wide range. Correspondingly, the temperatures for isothermal crystallization were chosen at similar supercoolings such that the crystallization process could be readily followed by our experimental methods.

2.2. ^1H low-resolution NMR FID

^1H time-domain NMR experiments were conducted on a Bruker Minispec mq20 spectrometer with a proton frequency of about 20 MHz ($B_0 \approx 0.47$ T) by using a static probe head to provide a mobility-based measure of absolute weight-based crystallinity by "proton counting". The temperature was controlled during the experiment via airflow regulated by a BVT3000 unit with an accuracy of about ±1 K and a gradient of up to 0.5 K across the sample. Prior to isothermal crystallization, the samples were molten 10–20 K above their melting temperature for

Table 1
Number of carbon–carbon bonds in the monomer along the backbone (N_{cc}), weight-average molecular weight (M_w), polydispersity index (PDI), glass transition temperature (T_g), melting temperature (T_m), mass crystallinity by NMR measurements ($X_{c,NMR}$), volume crystallinity by SAXS measurements ($X_{c,SAXS}$), density of crystalline and amorphous phases at room temperature (ρ_c, ρ_a), enthalpy of melting ($\Delta H_{m,100}$), and average monomer jump time ($\langle\tau_c\rangle$) of different polyesters. $T_m$was determined based on the maximum of melting peak position in the second heating scan of each polyester at 10 K min^{-1} by DSC. The corresponding DSC data are shown in Figure S1. $\Delta H_{m,100}$ was calculated from the NMR crystallinity values listed in Table S1 and the melting enthalpy measured by DSC in Figure S2. '*' indicates literature values, '–' denotes that data is not available, 'a' indicates data provided by suppliers.

	PGA	PLLA	P3HB	P4HB	PVL	PCL	PPDL
N_{cc}	1	1	2	3	4	5	14
M_w(kg mol^{-1})	100[a]	120[a]	–	848	190	188[a]	439
PDI	–	–	–	2.73	2	–	4.92
T_g* (°C)	40 [23]	50–60 [23]	0–27 [29–32]	−51 [33]	−66 [34]	−60 [35]	−23, −33 [36]
T_m (°C)	223	175	174	52	58	60* [37]	95
$X_{c,NMR}$ (wt.%)	60	–	–	35	52	–	47.9
$X_{c,SAXS}$ (vol.%)	44	60	70	36	52	–	46
ρ_c (g cm^{-3})	1.71 [38]	1.26 [39]	1.24 [40]	1.22 [41]	1.19 [42]	–	–
ρ_a (g cm^{-3})	1.45 [38]	1.25 [39]	1.18 [33]	1.21 [33]	–	–	–
$\Delta H^*_{m,100}$ (J g^{-1})	139 [43], 180, 202 [44], 183 [45]	104.5 [46]	146 [47]	–	182 [48]	157 [12]	227 [49], 233, 264 [36]
$\Delta H_{m,100}$ (J g^{-1})	129.3	–	–	96.9 ± 7.2	143.3 ± 4.7	–	211.7
$\langle\tau_c\rangle$* (s)	–	~3 [17]	~0.1 [10]	–	–	>1 [12]	–

~5 min as a compromise between the removal of thermal history and thermal degradation. Step cooling was performed starting from the sample's isothermal crystallization temperature at a rate of ~ 5 K min^{-1}, with an additional 10 min of equilibration before each free-induction decay (FID) measurement.

The 90° and 180° pulse lengths ranged from 1.5 to 1.8 μs and from 3.5 to 3.8 μs, respectively. Recycle delays (RD), which is the time between successive scans, was set between 4 to 10 s corresponding to about 5 times the ^{1}H T_1-relaxation time of the crystalline domain to ensure complete ^{1}H magnetization relaxation of the sample. As the instrument features a dead time of 15 μs, direct acquisition of the FID following a 90° pulse fails to capture the initial rapidly decaying crystalline component. To address this issue, the magic sandwich echo (MSE) [50] pulse technique was employed, which allows recovery of the early signal. Although the latter compensates for the dead time, its signal amplitude is reduced by pulse sequence imperfections and potential intermediate motions in the sample [7,51]. Therefore, only the shape parameters were extracted from the MSE-FID while the signal amplitudes were taken from the fits to the FIDs. Exemplary data of each sample are shown in Figure S3.

The crystallinity of the samples at each temperature was determined based on the relationship between strong ^{1}H-^{1}H dipole–dipole couplings and increasingly fast segmental dynamics in the interphase and the mobile amorphous phase. This means the amplitudes of FID components with short, intermediate and long dipolar-dephasing timescale (or T_2) reflect the crystal, interface and amorphous fractions, respectively [7]. The fitting equation based on this concept is,

$$I_{FID}(t) = A_c \cdot e^{-(a^2t^2/2)} \cdot \frac{\sin(b \cdot t)}{b \cdot t} + A_i \cdot e^{-(t/T^*_{2,i})^{\upsilon_i}} + A_a \cdot e^{-(t/T^*_{2,a})^{\upsilon_a}} \quad (1)$$

where t is time, $A_{c,i,a}$ represents the amplitude of the corresponding decaying component, $T^*_{2,i,a}$ and $\upsilon_{i,a}$ are the shape parameters (apparent T_2 and stretching exponent υ of the more mobile components, while a and b are the shape parameters of the crystalline part, where the so-called Abragamian function works well for polymers with only CH_2 groups along the main chain. A representative example of MSE-FID and FID curve fitting of each sample are shown in Figure S3. The crystallinity is calculated according to

$$X_c = \frac{A_c}{A_c + A_i + A_a} \cdot 100\% \quad (2)$$

2.3. ^{13}C Magic-angle spinning NMR spectroscopy

All ^{13}C MAS spectra measurements were performed using 400 MHz Bruker Avance III spectrometers equipped with double and triple resonance magic angle spinning (MAS) probes. The ^{13}C Larmor frequency was 100.6 MHz, and samples were spun at a MAS frequency of 10 kHz ± 3 Hz. The $\pi/2$-pulse power was set between 44 - 51 W for ^{1}H and 140 W for ^{13}C, corresponding to pulse lengths of approximately 3 μs. To enhance the inherently low sensitivity of ^{13}C nuclei, cross-polarization (CP) from ^{1}H was employed. A contact time (CT) of 1.5 ms was used to detect the (non-quantitative) full sample spectrum, while a short CT of 0.1 ms was chosen to minimize the contribution from amorphous segments, due to their lower ^{1}H-^{13}C polarization transfer efficiency, resulting in crystalline-phase dominated spectra. Additionally, direct polarization (DP) ^{13}C spectra with short recycle delay (RD) of 1 s were used to selectively detect mobile groups with fast T_1 relaxation, corresponding to mobile amorphous chains. ^{13}C spectra and peak assignments for each sample are shown in Figure S4.

2.4. T_1-Relaxation and diffusive exchange

The T_1-relaxation time of ^{13}C nuclei offers valuable insights into the molecular dynamics within semicrystalline polymers. In this work, ^{13}C T_1 measurements were carried out using a z-filtered pulse sequence after CP on the ^{13}C channel [6]. This technique ensures that the observed signal intensity, denoted as $I(\tau)$, decays to a well-defined zero with increasing relaxation delay τ. The measured decay of the signal can arise from either standard exponential T_1-relaxation or from a diffusive process transport of chains from the crystalline to the amorphous domain, where the T_1-relaxation is almost instantaneous [20]. A key feature of such diffusive behavior is a linear decay dependence of the I_τ on square root of time, $I_\tau \sim \sqrt{\tau}$. To differentiate between these two mechanisms, we plot the decay function $\log(1 - I_\tau/I_0)$ against

log(τ), where I_0 is the initial magnetization [10]. In this representation, the slope of 0.5 reflects a power-law dependence characteristic of chain diffusion, whereas exponential relaxation appears more non-linearly with initial slope of unity. This analytical approach enables clear identification and quantification of both diffusive exchange and T_1-relaxation.

2.5. SAXS

SAXS measurements were performed on a Kratky compact camera (Anton Paar GmbH, Graz, Austria) equipped with an X-ray optics (AXO Dresden GmbH, Germany), a temperature-controlled sample holder, and a 1D detector Mythen2 R 1K (Dectris, Switzerland). As the camera has a slit focus, the data had to be deconvoluted. This was achieved by applying the desmearing algorithm by Strobl [52].

The samples were quenched from their melt state (20–30 K higher than their T_m) to different isothermal crystallization temperatures in the Kratky camera. The exposure time for each measurement was 10 min. The analysis of the SAXS data is based on the interface distribution function (IDF or K"(z)), originally introduced by Ruland [53]. With the analysis, not only can the average crystalline layer (d_c) and amorphous layer (d_a) thickness be determined, but also the corresponding distribution widths, σ_c and σ_a, can be revealed, which are the essential morphological features telling difference between crystal-fixed polymers and crystal-mobile polymers. The detailed analysis procedure is described in our previous publications [12,14]. Examples of analysis of each polyester can be found in Figure S5-S11.

2.6. Dynamical mechanical analysis (DMA)

The shear modulus was measured with a rheometer Ares G2 equipped with heating chamber from TA instruments using a sample in stripe geometry (sample length between clamps 20 mm, width 10 mm, thickness 1.5 mm) at different temperatures but constant frequency of 10 rad s^{-1} and 0.1% strain. To prepare the samples with stripe geometry, all of them were heated 20–30 K above their melting temperatures for 10 min in a rectangular vacuum compression mold (MeltPrep, Graz, Austria) and cooled to different temperatures for isothermal crystallization according to Table S1. The cooling rate was estimated to be 5 K min^{-1}. Subsequently, the samples were transferred from the mold to the rheometer at room temperature.

2.7. Differential scanning calorimetry (DSC)

The melting temperatures and melting enthalpies of the samples were determined with a DSC 8000 from Perkin Elmer. Heating and cooling scans were conducted at a rate of 10 K min^{-1}. Prior to each measurement, the samples were heated 20 K to 30 K above their T_m for 10 min to erase thermal history.

3. Results and discussion

3.1. Comparison between timescales of ICD ($\langle\tau_c\rangle$) and layer crystallization (τ_{lc})

To investigate the dependence of semicrystalline morphology on the timescales of ICD ($\langle\tau_c\rangle$) relative to layer crystallization (τ_{lc}), we need to measure $\langle\tau_c\rangle$ and τ_{lc} of the selected aliphatic polyesters. Although it can be challenging to determine the exact $\langle\tau_c\rangle$ of the samples, due to the threshold of experimental techniques, we seek to at least estimate the range of $\langle\tau_c\rangle$ to quantify the relationship between the two timescales. Temperature-dependent ^{1}H NMR-free induction decay (FID) measurements were performed to examine the presence of fast ICD ($\langle\tau_c\rangle < 50$ µs) in the crystalline phase of the polyesters. In addition to probing fast ICD, the ^{1}H NMR-FID measurements provide a means to estimate the crystallinity (X_c) at different temperatures, which will be discussed at the end of this section. PLLA, P3HB and PCL were excluded from ^{1}H NMR-FID measurements because $\langle\tau_c\rangle$ of these polyesters is available in the literature [10,12,17]. If $\langle\tau_c\rangle < 200$ µs, the normalized crystalline FID line shape changes with temperatures [7]. However, the crystalline FID curves of each polyester, measured at different temperatures, superimpose (Figs. 2 and S12). This independence of the line shape on temperature indicates the absence of ICD on the timescale up to 200 µs at all measured temperatures.

As no fast ICD is present in PGA, P4HB, PVL and PPDL, we performed ^{13}C T_1-relaxation to access slower ICD, $\langle\tau_c\rangle$ up to 1 s, a timescale well within the sensitivity of this technique [4]. This approach probes long-range diffusive exchange between crystalline and amorphous phases. Therefore, prior to ^{13}C T_1-relaxation measurements, crystalline

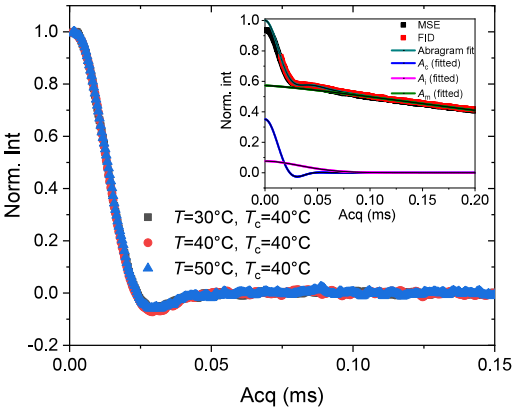

Fig. 2. Exemplary ^{1}H NMR-FID measurements of P4HB with intensity plotted vs. acquisition time at different crystallization temperatures. To illustrate the decomposition procedure the inset shows a set of full ^{1}H NMR-FID and MSE-FID curves, the complete fit and its three components: A_c(crystalline), A_i (intermediate) and A_m (amorphous). The main figure shows the crystalline component only. Crystalline components of other polyesters are shown in Figure S12.

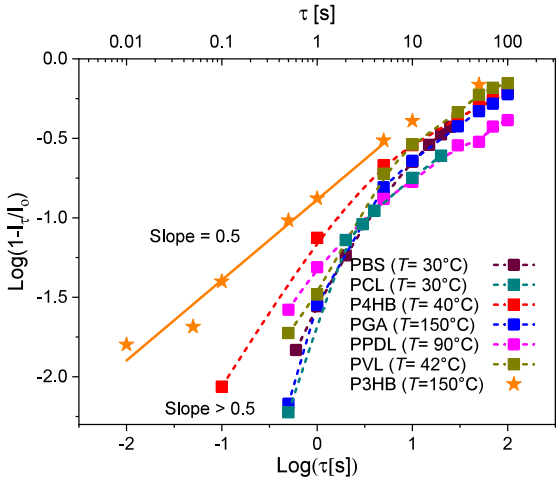

Fig. 3. ^{13}C T_1-relaxation data plotted as log(1 − I_τ/I_0) versus log(τ) on a crystalline peak (Figure S4) of isothermally crystallized PGA, P4HB, PVL, PCL and PPDL measured at the temperature indicated in the legend. The crystallization conditions correspond to Table S1. The data from PBS and P3HB are illustrated here as examples of typical crystal-fixed and crystal-mobile polymers, respectively [10,13]. The solid line is a linear fit with a slope of 0.5, indicative of ICD occurring on timescales faster than 1 s. The dashed lines serve as visual guides for the non-linearity of the initial data points, suggesting the absence of ICD within this timescale. The data for PBS, PCL and P3HB are taken from our previous publications [10,13].

and amorphous signals were distinguished based on selective ^{13}C NMR spectra (Figure S4). In rigid semicrystalline domains, ^{13}C T_1-relaxation typically shows a slow exponential decay ($\tau > 10$ s, τ is waiting time). However, as outlined in the Experimental Section 2.4, the presence of ICD enables magnetization exchange between phases, resulting in a faster decay of the crystalline peak intensity (I_τ) that follows a characteristic square-root dependence on the relaxation delay τ in the sub-second regime. This behavior is described by one-dimensional (1D) free-diffusion behavior [20,54–57]:

$$\frac{I_\tau}{I_0} = 1 - \frac{\sqrt{2D}}{d_c}\sqrt{\tau} \tag{3}$$

where D is the diffusion coefficient and d_c is the crystalline layer thickness. A logarithmic transformation of this equation allows for linearization:

$$\log(1 - \frac{I_\tau}{I_0}) = \frac{1}{2}\log(\tau) + \log\frac{\sqrt{2D}}{d_c} \tag{4}$$

Thus, a slope of 0.5 in the plot of $\log(1 - \frac{I_\tau}{I_0})$ versus $\log(\tau)$ is a hallmark of chain diffusion within the crystalline phase.

Fig. 3 presents this analysis for PGA, P3HB, P4HB, PVL, PCL, PPDL and polybutylene succinate (PBS). Among these, only P3HB, used here as a known crystal-mobile reference polymer [10], exhibits a slope of 0.5 at short τ, confirming the presence of ICD. The absence of such behavior in PGA, P4HB, PVL and PPDL suggests no detectable ICD up to 1 s. PBS and PCL are included as the reference polymers known to lack measurable ICD [12,13]. The presence of even slower ICD in the crystalline region is difficult to be probed by NMR measurements, although it might exist. However, a quantitative comparison of ICD turns out to be possible by SAXS measurement via observation of the crystal thickening rate, which is discussed separately in the following section.

The growth rate of spherulite (μ) of polyesters is measured at different crystallization temperatures by polarized optical microscopy. The layer crystallization time (τ_{lc}) is estimated from the spherulitic growth rate according to Eq. (5) [12].

$$\tau_{lc} = \frac{5\text{Å}}{\mu} \tag{5}$$

$\langle\tau_c\rangle$ of PGA, P4HB, PVL, PCL and PPDL (aliphatic polyesters without the CH_3 group as a side chain) is longer than τ_{lc}, while $\langle\tau_c\rangle$ of PLLA and P3HB (aliphatic polyesters with the CH_3 group as a side chain) is similar or even shorter than τ_{lc} (Figure S13). Therefore, the aliphatic polyesters without the CH_3 group as a side chain belong to the class of crystal-fixed polymers. The aliphatic polyesters with the CH_3 group as a side chain belong to the crystal-mobile polymers.

In addition, the crystallinity (X_c) measured by NMR indicates the presence of insertion crystallization in PGA, P4HB, PVL and PPDL. This is a morphological characteristic of crystal-fixed polymers [1,12,13], as illustrated in Fig. 4. The change of X_c of PCL versus temperatures can be found in Ref. [12]. X_c of all crystal-fixed polymers increases significantly with decreasing temperature, even after crystallization is complete at their corresponding crystallization temperatures. Furthermore, SAXS and wide-angle X-ray scattering (WAXS) results from these polymers can also qualitatively confirm the presence of insertion crystallization (Figure S14 and S15).

3.2. Semicrystalline morphology

To check the previously observed relation between ICD and the semicrystalline morphology, we characterized the semicrystalline morphology of the selected aliphatic polyesters by SAXS measurements. Fig. 5(a) shows the crystalline layer thickness (d_c), amorphous layer thickness (d_a) and their corresponding distribution widths, σ_c and σ_a of PGA, P4HB, PVL, PCL and PPDL, i.e. crystal-fixed polymers, at the corresponding crystallization temperatures. To facilitate comparison,

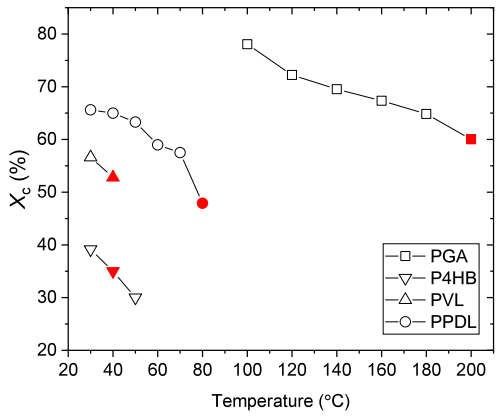

Fig. 4. Crystallinity (X_c) of PGA, P4HB, PVL and PPDL measured by ^1H NMR-FID versus temperature. The red data points were obtained at isothermal crystallization temperatures, while the black hollow data points were obtained during subsequent cooling or heating processes. Detailed crystallization conditions, including additional X_c obtained at other isothermal crystallization temperatures, are listed in Table S1.

only the corresponding results obtained at the end of the isothermal crystallization process at different temperatures are shown in Fig. 5(a). The complete morphological evolution of different polyesters during the course of the isothermal crystallization process at different temperatures can be found in Figure S16, S17 and S18. As shown in Fig. 5, d_c increases slightly with increasing isothermal crystallization temperature (T_c) for all five polyesters. d_c is always smaller than d_a or comparable to d_a(in the case of PVL). Importantly, the distribution width of the amorphous layer thickness (σ_a) of the 5 polymers is significantly broader than that of the crystalline layer thickness (σ_c). Please note that PGA possesses polymorphism, this study focuses only on its α form crystal [58,59]. Polymorphism of the other three polyesters has not been reported.

Fig. 5(b) presents the values of d_c, d_a and their corresponding distribution widths, σ_c and σ_a, for PLLA and P3HB (the crystal-mobile polymers) at the end of the crystallization process. Detailed time-dependent values can be found in Figures S19 and S20. d_c in contrast to above, of both polyesters increases with crystallization temperatures, while d_a is more or less independent of crystallization temperatures. At all crystallization temperatures, both polyesters show a greater value for d_c than for d_a, and a broader distribution width σ_c than σ_a. We are aware of polymorphism of both polyesters and present in this study only the semicrystalline morphology of the α-form crystals of both polyesters. This selection was achieved by choosing appropriate crystallization conditions [40,60–63].

Our measured values of d_c and d_a of all samples are consistent with available literature values [12,64–71], but, in addition, we provide a more complete analysis of the semicrystalline morphology by reporting the corresponding distribution widths. X_c values determined by SAXS ($X_c = d_c/(d_c + d_a) \cdot 100\%$) are in good agreements with those obtained from the NMR measurements (Table 1), with the exception of PGA, where discrepancies arise due to the large density difference between the crystalline and amorphous phases [38]. Furthermore, our study reveals the semicrystalline morphology of P4HB and PVL, which have not yet been reported in the literature. All of our results are consistent with the expectation based on our previous studies, which were based on a limited number of model polymers [4,12,13]: for crystal-fixed polymers, d_a is comparable to or greater than d_c and σ_a is broader than σ_c; conversely for crystal-mobile polymers, d_c is greater than d_a and σ_a is narrower than σ_c.

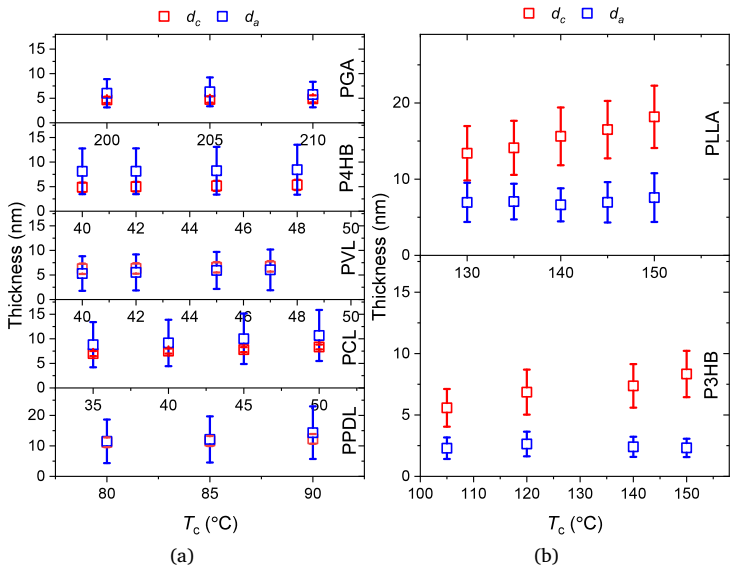

Fig. 5. (a) d_c and d_a of the five crystal-fixed polymers: PGA, P4HB, PVL, PCL and PPDL, measured at the corresponding isothermal crystallization temperatures based on the last points in Figures S16, S17 and S18. The error bars are the distribution width of d_a (in blue) and d_c (in red). The detailed SAXS analysis is illustrated in Figure S5, S6, S7 and S8. The assignment of d_c and d_a was based on the crystallinity measured by ^{1}H NMR-FID listed in Table S1 or the trend of change of d_c and d_a during crystallization (Figure S18 (a)). PCL data are reproduced from Ref. [12]. (b) d_c and d_a of PLLA and P3HB at different isothermal crystallization temperatures based on the last points in Figure S19 and S20. The error bars are the distribution width of d_a (in blue) and d_c (in red). The detailed SAXS analysis is illustrated in Figure S9 and S10. The assignment of d_c and d_a was based on crystallinity from the literature. P3HB and PLLA are known to have more than 50% crystallinity, according to Refs. [10,63].

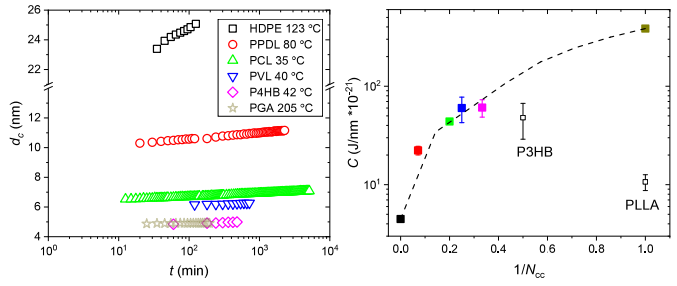

Fig. 6. (a) d_c of the different polymers during the isothermal crystallization process at the given temperatures. d_c values used for this comparison are taken during the secondary crystallization (Figure S16). PCL data are reproduced from Ref. [4]. (b) C values, i.e. energy barrier per unit length for thickening, of the polymers are calculated according to Eq. (7), based on the linear fitting in (a), and averaged for different crystallization temperatures. The dashed line is a guide for the eye. PLLA and P3HB data are obtained from Figure S20.

3.3. Quantitative comparison of ICDs of the crystal-fixed polymers

As previously observed in PCL [4], even polymers with ICD timescales ($\langle\tau_c\rangle$) longer than 1 s, i.e. not observable by NMR, can exhibit crystal thickening during secondary crystallization. This observation suggests that indeed on a longer timescale ICD takes place and motivates us to study their relative timescale of ICDs in different polyesters by comparing their crystal thickening processes during isothermal crystallization.

Fig. 6(a) illustrates the increase of crystalline layer thickness (d_c) of crystal-fixed polymers, plotted as a function of crystallization time on a logarithmic scale. High density polyethylene (HDPE), which is a crystal-mobile polymer, is also included, as the limiting case of an aliphatic polyesters with infinite N_{cc} (N_{cc} is the number of carbon–carbon bonds in the monomer along the backbone, namely the length of methylene sequence in the monomer). This treatment is justified for the investigation of crystallization as HDPE possesses similar chemical and crystal structure (chain conformation in the crystals and the crystal unit cell) as PGA, P4HB, PVL, PCL and PPDL [41,42,59,72–74]. A similar approach was also taken by other researchers [75].

In Fig. 6(a), d_c for all polymers increases linearly with the crystallization time on the logarithmic scale, and the crystal-thickening slope systematically decreases as N_{cc} decreases. The logarithmic dependence of d_c on the crystallization time has also observed in the literature [76–78]. This dependence is described by the differential equation (6) [76],

$$\frac{d(d_c)}{dt} = Ae^{-\frac{Cd_c}{kT}} \tag{6}$$

where k is the Bolzmann constant, A is the amplitude, T is the crystallization temperature, and C is an energy barrier per unit length. The solution of this equation is shown in Eq. (7). The slope of the crystal thickening is proportional to crystallization temperature T and inversely proportional to energy barrier per unit length C in the semi-logarithm plot,

$$d_c = \frac{2.3kT}{C} log\frac{A}{\frac{kT}{C}} + \frac{2.3kT}{C} log(t - t_0) \tag{7}$$

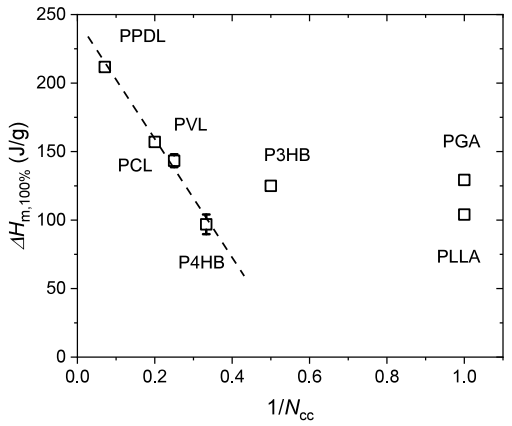

Fig. 7. $\Delta H_{m,100}$ of different polyesters. The results were determined based on melting enthalpy (DSC)/crystallinity (NMR). The error bar is the standard deviation. The dashed line is to guide the eyes. This linear relationship was proposed by other researchers with only available PPDL and PCL data [75]. $\Delta H_{m,100}$ of PLLA is reproduced from Ref. [46]. $\Delta H_{m,100}$ of PCL is reproduced from Ref. [12]. To facilitate the assignment of data points to the different samples, the sample names are indicated at the corresponding positions on the x-axis.

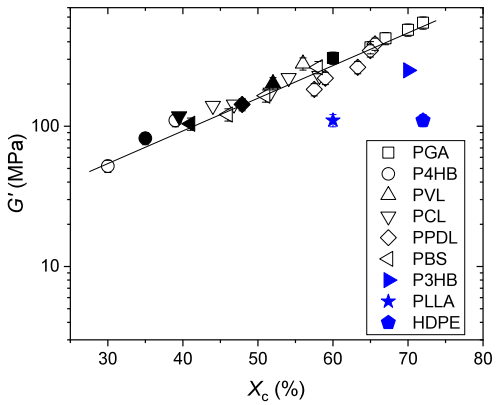

Fig. 8. Shear modulus (G') of different polymers versus crystallinity (X_c) at the temperatures above T_g and below T_m. The black solid data points represent G' of the crystal-sluggish polymers measured at the corresponding isothermal crystallization temperatures as illustrated in Fig. 4. The black hollow data points show G' of the crystal-sluggish polymers measured during the subsequent cooling and heating steps (Fig. 4 and S21). G' of the crystal-mobile polymers is shown in blue, which were measured at crystallization temperatures. Their crystallinities were also measured at the crystallization temperatures by SAXS measurement. All measurements were carried out at a frequency of 10 rad s^{-1} and a strain of 0.1%. The solid line is as a guide to the eye. PCL data are reproduced from Ref. [81]. The data of polybutylene succinate (PBS) are reproduced from Ref. [13]. G' of P3HB was calculated from the dynamic Young's modulus ($E = 3G$), measured at 140 °C, at a strain of 0.1% and a frequency of 1.59 Hz (tensile mode). The sample was isothermally crystallized at 140 °C for 40 min.

where t_0 is the starting time. The energy barrier C is plotted vs. $1/N_{cc}$ in Fig. 6(b). It increases systematically with $1/N_{cc}$, i.e. crystal thickening becomes slower, with decreasing distance between two adjacent ester groups and an increasing number of ester layers in the crystal. We attribute these effects to slower ICD, which becomes indirectly measurable in this way. Literature observations suggest that once this layered structure is disrupted, the polymers switch to the crystal-mobile class [18].

Based on these results, we recognize that the previous nomenclature for crystal-fixed polymer [20] is too simplistic. There is a clear need to refine and expand the classification of the crystal-fixed polymers. We propose the term "crystal-sluggish polymers" to describe the polymers that exhibit rather slow ICD while exhibiting crystal-fixed semicrystalline morphology. This term distinguishes them from strictly "crystal-fixed" polymers, which have no ICD. In the following text, we refer to all our polyesters showing the crystal-fixed semicrystalline morphology and non-detectable ICD by NMR measurements as crystal-sluggish polymers. Our results also provides a guideline for the molecular design of aliphatic polyesters with tailored ICD timescales. PLLA and P3HB are outliers in this comparison (Fig. 6(b)) because of their significantly different monomer structure (side group), chain conformation and unit cell [40,60], as well as no apparent presence of a layered structure [19]. We believe that this last fact is the reason, why they display faster ICD and therefore belong the class of crystal-mobile polymers.

3.4. Enthalpy of melting

Pepels et al. [75] introduced the hypothesis that the enthalpy of melting ($\Delta H_{m,100}$) decreases linearly with increasing ester content (proportional to $1/N_{cc}$ for the selected polyesters without side chain), based on two aliphatic polyesters (PCL and PPDL). We aim to examine its generality by using our samples with systematically varied ester content in a broad range and a more reliable experimental method for determining crystallinity, which results in reliable $\Delta H_{m,100}$. Fig. 7 shows the $\Delta H_{m,100}$ versus $1/N_{cc}$. Here, $\Delta H_{m,100}$ was calculated by dividing the melting enthalpies (measured by DSC) by the mass crystallinity (determined by NMR measurements), as listed in Table S1. Indeed, from PPDL to P4HB, with increasing $1/N_{cc}$, $\Delta H_{m,100}$ decreases linearly. With further increasing $1/N_{cc}$, P3HB, PLLA and PGA deviate from the linear trend and show higher $\Delta H_{m,100}$. Combining our results with those of Pepels et al. [75], which was based on rather low ester content (lower than PPDL), we confirm that the linear dependence of $\Delta H_{m,100}$ on ester content ($1/N_{cc}$) holds over an even broader range (from PPDL to P4HB) for aliphatic polyesters with all-trans chain conformation. The introduction of ester group into the crystals results in the energy penalty of the enthalpy of melting [75,79]. Here, we do not compare directly the results with Ref. [75], as Pepels et al. adopted few data points (only $\Delta H_{m,100}$ from PCL and PPDL), based on different experimental methods for the determination of crystallinity, the slope of linear trend of $\Delta H_{m,100}$ from their results is not comparable with ours. The observed deviation in P3HB, PLLA and PGA can be attributed to a few factors: their significantly different crystal unit cells (PLLA and P3HB) [40,60] and the presence of hydrogen bonding in PGA [65,80].

3.5. Shear modulus of the selected polyesters above T_g

Based on our extended knowledge of intracrystalline chain diffusion (ICD) and semicrystalline morphology of the selected polyesters, we aim to investigate shear modulus of the selected polyesters, which is highly related to ICD and semicrystalline morphology (X_c) [11,22] and crucial for practical applications [82–84].

The storage shear modulus (G') of all the selected aliphatic polyesters vs. X_c, is shown in Fig. 8. For the crystal-sluggish or crystal-fixed polymers, insertion crystallization [12,13] occurs during cooling and the additional crystals melt during heating. This phenomenon is qualitatively observed by SAXS and WAXS (Figure S14 and S15). Therefore, it is possible to measure their G' over a broad range of crystallinity. X_c of the crystal-sluggish polymers was quantitatively obtained using in-situ ^{1}H NMR-FID measurement conducted at different temperatures (Figs. 4). The solid data points represent measurement conducted at the corresponding isothermal crystallization temperatures, while the hollow data points correspond to subsequent heating and cooling steps. G' of the crystal-sluggish polymers, subjected to the same thermal history as during the NMR measurement, was measured by the rheometer at the frequency of 10 rad s^{-1} and the strain amplitude of

0.1% (Figure S21). X_c and G' of the crystal-mobile polymers were obtained using SAXS measurements and the rheometer at the same temperatures. On a logarithmic scale, G' of all crystal-sluggish polymers (black data points) shows a linear dependence on X_c, indicating an exponential relationship ($G' \sim e^{AX_c}$). In contrast, the G' values of crystal-mobile polymers (blue data points) do not follow this exponential trend and are systematically lower than the extrapolated dependence. We rely on NMR-derived crystallinity values for all crystal-sluggish polymers because our SAXS analysis is not applicable for the insertion crystallization during the heating and cooling steps used in those measurements.

The exponential dependence of G' of the crystal-sluggish polymers on X_c indicates that X_c is the dominant factor governing the modulus. As we cannot provide a derivation for the exponential dependence, we report it here as a mere observation. Nevertheless, this dependence has also been reported by other researchers for the case of polyethylene (PE) [22]. However, in the case of PE, it is difficult to decouple the contributions of X_c and d_c to the modulus, since its X_c is typically proportional to d_c. With the semicrystalline morphology information from the crystal-sluggish polymers (Figure S22), on the other hand we find no clear dependence of G' on d_c. This allows us to exclude d_c as a major factor affecting modulus in these systems, despite its consideration as a key parameter by other researchers [85,86].

Furthermore, the deviation observed in crystal-mobile polymers is attributed to the measurement frequency of $10\,\mathrm{rad\,s^{-1}}$, which falls within the timescale of the α_c-relaxation associated with ICD [10,17,20]. As a result, the relaxation process reduces the measured value of G', in agreement with the observations reported in the literature [10,22].

4. Conclusion

In conclusion, the selected aliphatic polyesters exhibit semicrystalline morphologies that are in agreement with our prediction based on our previous studies [12], regarding the relation between timescales of intracrystalline chain diffusion ($\langle\tau_c\rangle$) and layer crystallization (τ_{lc}).

Our SAXS-based approach enables the quantitative analysis of crystal thickening and the comparison of ICD timescale by comparison of the C-value (energy barrier per unit length), for crystal-sluggish polymers, which is not possible via NMR. From HDPE to PPDL, ICD slows down due to the formation of the layered structure of the ester groups in the crystals. When the concentration of the ester layers per unit length (d_c) increases, i.e. with decreasing N_{cc} (from PPDL to PGA), the timescale of ICD slows down. Based on our observations, we propose that the established distinction between crystal-fixed and crystal-mobile polymers [5] should be further refined and expanded. Polymers with ICD that is too slow to significantly affect crystallization and therefore exhibit a crystal-fixed morphology but show crystal thickening during secondary crystallization, we suggest to call crystal-sluggish polymers. The term crystal-fixed then remains for the limit of infinitely slow or non-existing ICD. PGA or PBS [13] come close to this limit.

Furthermore, the enthalpy of melting ($\Delta H_{m,100}$) of the polyesters decreases linearly with increasing ester content ($1/N_{cc}$), from PPDL to P4HB, due to the incorporation of ester groups in the polymer crystals.

Lastly, we reveal an exponential dependence of shear modulus (G') of polymers on crystallinity (X_c) measured at a frequency, $\omega \gg 1/\langle\tau_c\rangle$, in the temperature range between T_g and T_m. By comparing G' values of polymers with different d_c, we exclude d_c as a dominant factor influencing modulus in crystal-sluggish polymers.

This study provides an advance in fundamental understanding from chemical structure (N_{cc}, side chain), morphological features to linear mechanical properties in the hope of supporting further development of aliphatic polyesters, which are a promising candidate for replacement of commodity plastics. However, these materials still face limitations in mechanical performance, particularly in non-linear regimes. We hope this work lays the ground for further investigations of the influence of ICD on nonlinear mechanical properties.

CRediT authorship contribution statement

Qiang Yu: Writing – original draft, Visualization, Validation, Investigation, Formal analysis, Data curation, Conceptualization. **Afiq Anuar:** Writing – original draft, Visualization, Validation, Formal analysis, Data curation. **Aaron Miller:** Investigation. **Sharifa Abdullaeva:** Investigation. **Katalee Jariyavidyanont:** Investigation. **Albrecht Petzold:** Supervision, Software, Methodology. **Svenja Stürmer:** Resources. **Felix Scheliga:** Resources, Investigation. **Kay Saalwächter:** Writing – review & editing, Supervision, Resources, Methodology, Funding acquisition, Conceptualization. **Thomas Thurn-Albrecht:** Writing – review & editing, Supervision, Resources, Project administration, Methodology, Funding acquisition, Conceptualization.

Declaration of competing interest

The authors declare that they have no known competing financial interests or personal relationships that could have appeared to influence the work reported in this paper.

Acknowledgments

The authors thank the Deutsche Forschungsgemeinschaft (DFG), Germany for financial support in the framework of the SFB-TRR 102 (project-ID 189853844), project A1, and for funding of NMR instrumentation (INST 271/446-1 FUGG). Furthermore, the authors acknowledge K. Herfurt for technical help with DSC measurements, V. Vulchi for help in partial SAXS measurements of PLLA, and Prof. Manfred Zinn for the synthesis of P4HB.

Appendix A. Supplementary data

Supplementary material related to this article can be found online at https://doi.org/10.1016/j.polymer.2025.129131.

Data availability

The data published in the Figures of this article are available under the DOI https://doi.org/10.5281/zenodo.15648710.

References

[1] G. Strobl, The physics of polymers. Concepts for understanding their structures and behavior, 3., rev. and expanded ed., Springer, Berlin [u.a.], 2007, http://dx.doi.org/10.1007/978-3-540-68411-4, XIII, 518 S..
[2] R.H. Boyd, Relaxation processes in crystalline polymers: experimental behaviour - a review, Polymer 26 (3) (1985) 323–347.
[3] R.H. Boyd, Relaxation processes in crystalline polymers: Molecular interpretation - a review, Polymer 26 (8) (1985) 1123–1133, http://dx.doi.org/10.1016/0032-3861(85)90240-X.
[4] M. Schulz, M. Schäfer, K. Saalwächter, T. Thurn-Albrecht, Competition between crystal growth and intracrystalline chain diffusion determines the lamellar thickness in semicrystalline polymers, Nat. Commun. 13 (1) (2022) 119, http://dx.doi.org/10.1038/s41467-021-27752-0.
[5] W. Hu, K. Schmidt-Rohr, Polymer ultradrawability: the crucial role of alpha-relaxation chain mobility in the crystallites, Acta Polym. 50 (8) (1999) 271–285.
[6] D.A. Torchia, The measurement of proton-enhanced carbon-13 T1 values by a method which suppresses artifacts, J. Magn. Reson. (1969) 30 (3) (1978) 613–616, http://dx.doi.org/10.1016/0022-2364(78)90288-3.
[7] K. Schäler, M. Roos, P. Micke, Y. Golitsyn, A. Seidlitz, T. Thurn-Albrecht, H. Schneider, G. Hempel, K. Saalwächter, Basic principles of static proton low-resolution spin diffusion NMR in nanophase-separated materials with mobility contrast, Solid State Nucl. Magn. Reson. 72 (2015) 50–63.
[8] R. Kurz, A. Achilles, W. Chen, M. Schäfer, A. Seidlitz, Y. Golitsyn, J. Kressler, W. Paul, G. Hempel, T. Miyoshi, T. Thurn-Albrecht, K. Saalwächter, Intracrystalline jump motion in poly(ethylene oxide) lamellae of variable thickness: A comparison of NMR methods, Macromolecules 50 (10) (2017) 3890–3902, http://dx.doi.org/10.1021/acs.macromol.7b00843.
[9] Y. Men, J. Rieger, H.F. Endeler, D. Lilge, Mechanical alpha-process in polyethylene, Macromolecules 36 (13) (2003) 4689–4691.

[10] A. Anuar, Q. Yu, K. Jariyavidyanont, A. Petzold, R. Androsch, T. Thurn-Albrecht, K. Saalwächter, Poly-3-hydroxybutyrate, a crystal-mobile biodegradable polyester, Macromolecules 57 (17) (2024) 8507–8518, http://dx.doi.org/10.1021/acs.macromol.4c00938.

[11] S. Humbert, O. Lame, R. Seguela, G. Vigier, A re-examination of the elastic modulus dependence on crystallinity in semi-crystalline polymers, Polymer 52 (21) (2011) 4899–4909, http://dx.doi.org/10.1016/j.polymer.2011.07.060.

[12] M. Schulz, A. Seidlitz, R. Kurz, R. Barenwald, A. Petzold, K. Saalwachter, T. Thurn-Albrecht, The underestimated effect of intracrystalline chain dynamics on the morphology and stability of semicrystalline polymers, Macromolecules 51 (21) (2018) 8377–8385, http://dx.doi.org/10.1021/acs.macromol.8b01102.

[13] Q. Yu, A. Anuar, A. Petzold, J. Balko, K. Saalwächter, T. Thurn-Albrecht, The semicrystalline morphology of polybutylene succinate supports a general scheme based on intracrystalline dynamics, Macromol. Chem. Phys. n/a (n/a) (2023) 2200459, http://dx.doi.org/10.1002/macp.202200459.

[14] A. Seidlitz, T. Thurn-Albrecht, Small-angle X-ray scattering for morphological analysis of semicrystalline polymers, in: Q. Guo (Ed.), Polymer Morphology, Wiley & Sons, Hoboken, 2016, pp. 151–164, http://dx.doi.org/10.1002/9781118892756.ch9.

[15] T. Albrecht, G. Strobl, Temperature-dependent crystalline-amorphous structures in linear polyethylene - surface melting and the thickness of the amorphous layers, Macromolecules 28 (17) (1995) 5827–5833, http://dx.doi.org/10.1021/ma00121a020.

[16] U.W. Gedde, Polymer Physics, 1. ed, Chapman and Hall, London [u.a.], 1995, p. X, 298 S.

[17] W. Chen, W. Zhou, Y. Makita, S. Wang, S. Yuan, T. Konishi, T. Miyoshi, Characterization of the slow molecular dynamics of poly(l-lactic acid) in α and $\alpha\prime$ phases, in a glassy state, and in a complex with poly(d-lactic acid) by solid-state NMR, Macromol. Chem. Phys. 219 (3) (2018) 1700451, http://dx.doi.org/10.1002/macp.201700451.

[18] M.P.F. Pepels, L.E. Govaert, R. Duchateau, Influence of the main-chain configuration on the mechanical properties of linear aliphatic polyesters, Macromolecules 48 (16) (2015) 5845–5854, http://dx.doi.org/10.1021/acs.macromol.5b01089.

[19] Y. Song, Z. Ma, P. Yang, X. Zhang, X. Lyu, K. Jiang, W. Zhang, Single-molecule force spectroscopy study on force-induced melting in polymer single crystals: The chain conformation matters, Macromolecules 52 (3) (2019) 1327–1333, http://dx.doi.org/10.1021/acs.macromol.8b02702.

[20] K. Schmidt-Rohr, H. Spiess, Chain diffusion between crystalline and amorphous regions in polyethylene detected by 2D exchange C-13 nmr, Macromolecules 24 (19) (1991) 5288–5293.

[21] S.F. Marxsen, M. Häußler, S. Mecking, R.G. Alamo, Isothermal step thickening in a long-spaced aliphatic polyester, Polymer 191 (2020) 122282, http://dx.doi.org/10.1016/j.polymer.2020.122282.

[22] B. Christ, C. Fisher, P. Howard, Mechanical properties of model polyethylenes: Tensile elastic modulus and yield stress, Macromolecules 22 (4) (1989) 1709–1718.

[23] Y. Ikada, H. Tsuji, Biodegradable polyesters for medical and ecological applications, Macromol. Rapid Commun. 21 (3) (2000) 117–132, http://dx.doi.org/10.1002/(SICI)1521-3927(20000201)21:3<117::AID-MARC117>3.0.CO;2-X.

[24] D.P. Martin, S.F. Williams, Medical applications of poly-4-hydroxybutyrate: a strong flexible absorbable biomaterial, Biochem. Eng. J. 16 (2) (2003) 97–105, http://dx.doi.org/10.1016/S1369-703X(03)00040-8.

[25] T.A. Swetha, V. Ananthi, A. Bora, N. Sengottuvelan, K. Ponnuchamy, G. Muthusamy, A. Arun, A review on biodegradable polylactic acid (PLA) production from fermentative food waste - its applications and degradation, Int. J. Biiol. Macromol. 234 (2023) 123703, http://dx.doi.org/10.1016/j.ijbiomac.2023.123703.

[26] G.Q. Chen, Q. Wu, Y.K. Jung, S.Y. Lee, 3.21 - PHA/phb, in: M. Moo-Young (Ed.), Comprehensive Biotechnology (Second Edition), Academic Press, Burlington, 2011, pp. 217–227, http://dx.doi.org/10.1016/B978-0-08-088504-9.00179-3.

[27] S.M. Satti, A.A. Shah, Polyester-based biodegradable plastics: an approach towards sustainable development, Lett. Appl. Microbiol. 70 (6) (2020) 413–430, http://dx.doi.org/10.1111/lam.13287.

[28] A. Nandakumar, J.-A. Chuah, K. Sudesh, Bioplastics: A boon or bane? Renew. Sustain. Energy Rev. 147 (2021) 111237, http://dx.doi.org/10.1016/j.rser.2021.111237.

[29] G.-Q. Chen, Production and applications of microbial polyhydroxyalkanoates, in: E. Chiellini, R. Solaro (Eds.), Biodegradable Polymers and Plastics, Springer US, 2003, pp. 155–166, http://dx.doi.org/10.1007/978-1-4419-9240-6_11.

[30] C. Schick, A. Wurm, A. Mohamed, Vitrification and devitrification of the rigid amorphous fraction of semicrystalline polymers revealed from frequency-dependent heat capacity, Colloid Polym. Sci. 279 (8) (2001) 800–806.

[31] A. Czerniecka, A. Magoń, J. Schliesser, B.F. Woodfield, M. Pyda, Heat capacity of poly(3-hydroxybutyrate), J. Chem. Thermodyn. 73 (2014) 76–84, http://dx.doi.org/10.1016/j.jct.2013.10.020.

[32] Z. Wei, L. Liu, M. Qi, Synthesis and characterization of homo- and co-polymers of (r,s)-β-butyrolactone and γ-butyrolactone or β-valerolactone initiated with cyclic tin alkoxide, React. Funct. Polym. 66 (12) (2006) 1411–1419, http://dx.doi.org/10.1016/j.reactfunctpolym.2006.04.004.

[33] C. Utsunomia, Q. Ren, M. Zinn, Poly(4-hydroxybutyrate): Current state and perspectives, Front. Bioeng. Biotechnol. 8 (2020) http://dx.doi.org/10.3389/fbioe.2020.00257.

[34] B. Lebedev, A. Yevstropov, Thermodynamic properties of polylactones, Die Makromol. Chem. 185 (6) (1984) 1235–1253, http://dx.doi.org/10.1002/macp.1984.021850617.

[35] A. Fernández-Tena, R.A. Pérez-Camargo, O. Coulembier, L. Sangroniz, N. Aranburu, G. Guerrica-Echevarria, G. Liu, D. Wang, D. Cavallo, A.J. Müller, Effect of molecular weight on the crystallization and melt memory of poly(caprolactone) (PCL), Macromolecules 56 (12) (2023) 4602–4620, http://dx.doi.org/10.1021/acs.macromol.3c00234, URL https://doi.org/10.1021/acs.macromol.3c00234.

[36] P. Skoglund, Å. Fransson, Thermophysical properties of polypentadecanolactone, Polymer 39 (10) (1998) 1899–1906, http://dx.doi.org/10.1016/S0032-3861(97)00473-4.

[37] A.-K. Flieger, M. Schulz, T. Thurn-Albrecht, Interface-induced crystallization of polycaprolactone on graphite via first-order prewetting of the crystalline phase, Macromolecules 51 (1) (2018) 189–194, http://dx.doi.org/10.1021/acs.macromol.7b02113.

[38] J.E. Mark, Polymer Data Handbook, second ed., Oxford University Press Inc., New York u.a., 2009, pp. 1–1012, http://dx.doi.org/10.1021/ja907879q.

[39] K. Jariyavidyanont, A. Janke, Q. Yu, T. Thurn-Albrecht, R. Androsch, Lamellar morphology of disorder $\alpha\prime$-crystals of poly(l-lactic acid), Cryst. Growth Des. (2024) http://dx.doi.org/10.1021/acs.cgd.3c01498.

[40] M. Yokouchi, Y. Chatani, H. Tadokoro, K. Teranishi, H. Tani, Structural studies of polyesters: 5. Molecular and crystal structures of optically active and racemic poly (β-hydroxybutyrate), Polymer 14 (6) (1973) 267–272, http://dx.doi.org/10.1016/0032-3861(73)90087-6.

[41] F. Su, T. Iwata, K. Sudesh, Y. Doi, Electron and X-ray diffraction study on poly(4-hydroxybutyrate), Polymer 42 (21) (2001) 8915–8918, http://dx.doi.org/10.1016/s0032-3861(01)00412-8.

[42] Y. Furuhashi, P. Sikorski, E. Atkins, T. Iwata, Y. Doi, Structure and morphology of the aliphatic polyester poly(δ-valerolactone) in solution-grown, chain-folded lamellar crystals, J. Polym. Sci. Part B: Polym. Phys. 39 (21) (2001) 2622–2634, http://dx.doi.org/10.1002/polb.10024.

[43] D. Cohn, H. Younes, G. Marom, Amorphous and crystalline morphologies in glycolic acid and lactic acid polymers, Polymer 28 (12) (1987) 2018–2022, http://dx.doi.org/10.1016/0032-3861(87)90035-8.

[44] K. Chujo, H. Kobayashi, J. Suzuki, S. Tokuhara, M. Tanabe, Ring-opening polymerization of glycolide, Die Makromol. Chem. 100 (1) (1967) 262–266, http://dx.doi.org/10.1002/macp.1967.021000128.

[45] C. Nakafuku, H. Yoshimura, Melting parameters of poly(glycolic acid), Polymer 45 (11) (2004) 3583–3585, http://dx.doi.org/10.1016/j.polymer.2004.03.041.

[46] K. Jariyavidyanont, M. Du, Q. Yu, T. Thurn-Albrecht, C. Schick, R. Androsch, Bulk enthalpy of melting of poly (l-lactic acid) (PLLA) determined by fast scanning chip calorimetry, Macromol. Rapid Commun. n/a (n/a) (2022) 2200148, http://dx.doi.org/10.1002/marc.202200148.

[47] P.J. Barham, A. Keller, E.L. Otun, P.A. Holmes, Crystallization and morphology of a bacterial thermoplastic: poly-3-hydroxybutyrate, J. Mater. Sci. 19 (9) (1984) 2781–2794, http://dx.doi.org/10.1007/bf01026954.

[48] A.A. Yevstropov, B.V. Lebedev, T.G. Kulagina, N.K. Lebedev, The calorimetric study in the 13 ·8–340°k range of δ-valerolactone, its polymer, and of the δ-valerolactone polymerization, Polym. Sci. U.S.S.R. 24 (3) (1982) 628–636, http://dx.doi.org/10.1016/0032-3950(82)90053-3.

[49] J. Cai, B.S. Hsiao, R.A. Gross, Polypentadecalactone prepared by lipase catalysis: crystallization kinetics and morphology, Polym. Int. 58 (8) (2009) 944–953, http://dx.doi.org/10.1002/pi.2624.

[50] W.K. Rhim, A. Pines, J.S. Waugh, Time-reversal experiments in dipolar-coupled spin systems, Phys. Rev. B 3 (3) (1971) 684–696, http://dx.doi.org/10.1103/PhysRevB.3.684.

[51] R. Bärenwald, Y. Champouret, K. Saalwächter, K. Schäler, Determination of chain flip rates in poly(ethylene) crystallites by solid-state low-field H-1 NMR for two different sample morphologies, J. Phys. Chem. B 116 (43) (2012) 13089–13097.

[52] G. Strobl, A new method for evaluating slit-smeared small angle X-Ray scattering data, Acta Crystallogr. Sect. Crystal Phys. Diffr. Theor. Gen. Crystallogr. A 26 (1970) 367–375.

[53] W. Ruland, The evaluation of the small-angle scattering of lamellar two-phase systems by means of interface distribution functions, Colloid Polym. Sci. 255 (5) (1977) 417–427.

[54] R. Bärenwald, S. Goerlitz, R. Godehardt, A. Osichow, Q. Tong, M. Krumova, S. Mecking, K. Saalwächter, Correction to local flips and chain motion in polyethylene crystallites: A comparison of melt-crystallized samples, reactor powders, and nanocrystals (vol 47, pg 5163, 2014), Macromolecules 47 (21) (2014) 7677–7678.

[55] Y. Yao, R. Graf, H. Spiess, D. Lippits, S. Rastogi, Morphological differences in semicrystalline polymers: Implications for local dynamics and chain diffusion, Phys. Rev. E 76 (6) (2007) 060801–+, http://dx.doi.org/10.1103/PhysRevE.76.060801.

[56] Y. Yao, R. Graf, H. Spiess, S. Rastogi, Influence of crystal thickness and topological constraints on chain diffusion in linear polyethylene, Macromol. Rapid Commun. 30 (13) (2009) 1123–1127, http://dx.doi.org/10.1002/marc.200900114.

[57] D.E. Axelson, L. Mandelkern, R. Popli, P. Mathieu, Carbon-13 NMR of polyethylenes: Correlation of the crystalline component T1 with structure, J. Polym. Sci.: Polym. Phys. Ed. 21 (11) (1983) 2319–2335, http://dx.doi.org/10.1002/pol.1983.180211109.

[58] D. Niu, H. Wang, Y. Ma, P. Xu, J. Li, W. Yang, T. Liu, K. Tashiro, P.J. Lemstra, P. Ma, A β-form crystal modification of poly(glycolic acid): Formation, stabilization, and β–α transition, Macromolecules 56 (16) (2023) 6316–6327, http://dx.doi.org/10.1021/acs.macromol.3c01168.

[59] Y. Chatani, K. Suehiro, Y. Ôkita, H. Tadokoro, K. Chujo, Structural studies of polyesters. I. Crystal structure of polyglycolide, Die Makromol. Chem. 113 (1) (1968) 215–229, http://dx.doi.org/10.1002/macp.1968.021130119.

[60] P. De Santis, A.J. Kovacs, Molecular conformation of poly(s-lactic acid), Biopolymers 6 (3) (1968) 299–306, http://dx.doi.org/10.1002/bip.1968.360060305.

[61] J. Puiggali, Y. Ikada, H. Tsuji, L. Cartier, T. Okihara, B. Lotz, The frustrated structure of poly(l-lactide), Polymer 41 (25) (2000) 8921–8930, http://dx.doi.org/10.1016/S0032-3861(00)00235-4.

[62] T. Iwata, M. Fujita, Y. Aoyagi, Y. Doi, T. Fujisawa, Time-resolved X-ray diffraction study on poly[(r)-3-hydroxybutyrate] films during two-step-drawing: generation mechanism of planar zigzag structure, Biomacromolecules 6 (3) (2005) 1803–1809, http://dx.doi.org/10.1021/bm050152s.

[63] K. Jariyavidyanont, Q. Yu, A. Petzold, T. Thurn-Albrecht, R. Glüge, H. Altenbach, R. Androsch, Young's modulus of the different crystalline phases of poly (l-lactic acid), J. Mech. Behav. Biomed. Mater. 137 (2023) 105546, http://dx.doi.org/10.1016/j.jmbbm.2022.105546.

[64] H. Montes de Oca, I.M. Ward, R.A. Chivers, D.F. Farrar, Structure development during crystallization and solid-state processing of poly(glycolic acid), J. Appl. Polym. Sci. 111 (2) (2009) 1013–1018, http://dx.doi.org/10.1002/app.29000.

[65] F. Nishimura, H. Hoshina, Y. Ozaki, H. Sato, Isothermal crystallization of poly(glycolic acid) studied by terahertz and infrared spectroscopy and SAXS/WAXD simultaneous measurements, Polym. J. 51 (2) (2019) 237–245, http://dx.doi.org/10.1038/s41428-018-0150-7.

[66] C. Yu, J. Bao, Q. Xie, G. Shan, Y. Bao, P. Pan, Crystallization behavior and crystalline structural changes of poly(glycolic acid) investigated via temperature-variable WAXD and ftir analysis, CrystEngComm 18 (40) (2016) 7894–7902, http://dx.doi.org/10.1039/C6CE01623E.

[67] J. Cai, C. Liu, M. Cai, J. Zhu, F. Zuo, B.S. Hsiao, R.A. Gross, Effects of molecular weight on poly(ω-pentadecalactone) mechanical and thermal properties, Polymer 51 (5) (2010) 1088–1099, http://dx.doi.org/10.1016/j.polymer.2010.01.007.

[68] H. Abe, M. Harigaya, Y. Kikkawa, T. Tsuge, Y. Doi, Crystal growth and solid-state structure of poly(lactide) stereocopolymers, Biomacromolecules 6 (1) (2005) 457–467, http://dx.doi.org/10.1021/bm049497l.

[69] T.-Y. Cho, G. Strobl, Temperature dependent variations in the lamellar structure of poly(l-lactide), Polymer 47 (4) (2006) 1036–1043, http://dx.doi.org/10.1016/j.polymer.2005.12.027.

[70] T. Van Nguyen, T. Nagata, K. Noso, K. Kaji, H. Masunaga, T. Hoshino, T. Hikima, S. Sakurai, K. Yamamoto, Y. Miura, T. Aoki, H. Yamane, S. Sasaki, Effect of the 3-hydroxyhexanoate content on melt-isothermal crystallization behavior of microbial poly(3-hydroxybutyrate-co-3-hydroxyhexanoate), Macromolecules 54 (18) (2021) 8738–8750, http://dx.doi.org/10.1021/acs.macromol.1c01177.

[71] H.-J. Chiu, J.-W. You, Lamellar morphology of poly(3-hydroxybutyrate)/poly(ethylene oxide) blends as studied via small angle X-ray scattering, J. Polym. Res. 10 (2) (2003) 79–85, http://dx.doi.org/10.1023/A:1024907230151.

[72] Y. Chatani, Y. Okita, H. Tadokoro, Y. Yamashita, Structural studies of polyesters .3. Crystal structure of poly-epsilon-caprolactone, Polym. J. 1 (5) (1970) 555–562.

[73] M. Gazzano, V. Malta, M.L. Focarete, M. Scandola, R.A. Gross, Crystal structure of poly(ω-pentadecalactone), J. Polym. Sci. Part B: Polym. Phys. 41 (10) (2003) 1009–1013, http://dx.doi.org/10.1002/polb.10419.

[74] G. Davis, R. Eby, J. Colson, Thermal expansion of polyethylene unit cell - effect of lamella thickness, J. Appl. Phys. 41 (11) (1970) 4316–4326, http://dx.doi.org/10.1063/1.1658462.

[75] M.P.F. Pepels, M.R. Hansen, H. Goossens, R. Duchateau, From polyethylene to polyester: Influence of ester groups on the physical properties, Macromolecules 46 (19) (2013) 7668–7677, http://dx.doi.org/10.1021/ma401403x.

[76] J.J. Weeks, Melting temperature and change of lamellar thickness with time for bulk polyethylene, J Res Natl Bur Stand A Phys Chem 67A (5) (1963) 441–451, http://dx.doi.org/10.6028/jres.067A.046.

[77] E. Fischer, Zusammenhänge zwischen der kolloidstruktur kristalliner hochpolymerer und ihrem schmelz- und rekristallisationsverhalten, Kolloid Zeitschrift Zeitschrift Polym. 231 (1–2) (1969) 458–503.

[78] H. Marand, Z. Huang, Isothermal lamellar thickening in linear polyethylene: correlation between the evolution of the degree of crystallinity and the melting temperature, Macromolecules 37 (17) (2004) 6492–6497, http://dx.doi.org/10.1021/ma0497198.

[79] B. Crist, Thermodynamics of statistical copolymer melting, Polymer 44 (16) (2003) 4563–4572, http://dx.doi.org/10.1016/S0032-3861(03)00331-8.

[80] H. Sato, M. Miyada, S. Yamamoto, K. Raghunatha Reddy, Y. Ozaki, C–h···o (ether) hydrogen bonding along the (110) direction in polyglycolic acid studied by infrared spectroscopy, wide-angle X-ray diffraction, quantum chemical calculations and natural bond orbital calculations, RSC Adv. 6 (20) (2016) 16817–16823, http://dx.doi.org/10.1039/C5RA19900J.

[81] Z. Wang, M. Schaller, A. Petzold, K. Saalwächter, T. Thurn-Albrecht, How entanglements determine the morphology of semicrystalline polymers, Proc. Natl. Acad. Sci. 120 (27) (2023) e2217363120, http://dx.doi.org/10.1073/pnas.2217363120.

[82] X. Zhao, K. Cornish, Y. Vodovotz, Narrowing the gap for bioplastic use in food packaging: An update, Environ. Sci. Technol. 54 (8) (2020) 4712–4732, http://dx.doi.org/10.1021/acs.est.9b03755.

[83] M. Peydayesh, M. Bagnani, R. Mezzenga, Sustainable bioplastics from amyloid fibril-biodegradable polymer blends, ACS Sustain. Chem. Eng. 9 (35) (2021) 11916–11926, http://dx.doi.org/10.1021/acssuschemeng.1c03937.

[84] T. Fujimaki, Processability and properties of aliphatic polyesters, 'bionolle', synthesized by polycondensation reaction, Polym. Degrad. Stab. 59 (1) (1998) 209–214, http://dx.doi.org/10.1016/S0141-3910(97)00220-6.

[85] K. Molina-Besch, H. Keszleri, Exploring the industrial perspective on biobased plastics in food packaging applications – insights from Sweden, Sustain. Prod. Consum. 35 (2023) 72–84, http://dx.doi.org/10.1016/j.spc.2022.10.018.

[86] A. Zarbali, B. Pinke, A. Menyhárd, Robustness study of a tensile modulus prediction model for semicrystalline polymers, Period. Polytech. Chem. Eng. 67 (2) (2023) 232–241, http://dx.doi.org/10.3311/PPch.20991.